The transcriptional regulator MEIS2 sets up the ground state for palatal osteogenesis in mice

Received for publication, January 18, 2020, and in revised form, March 10, 2020 Published, Papers in Press, March 13, 2020, DOI 10.1074/jbc.RA120.012684

Linyan Wang[‡§1], Qinghuang Tang[§], Jue Xu[§¶], Hua Li[§], Tianfang Yang[§], Liwen Li[§], Ondrej Machon[‖2], Tao Hu[‡], and YiPing Chen[§3]

From the [‡]State Key Laboratory of Oral Diseases, Department of Preventive Dentistry, West China Hospital of Stomatology, Sichuan University, Chengdu 610041, Sichuan, China, the [§]Department of Cell and Molecular Biology, Tulane University, New Orleans, Louisiana 70118, the [¶]West China School of Public Health and West China Fourth Hospital, Sichuan University, Chengdu 610041, Sichuan, China, and the [‖]Department of Developmental Biology, Institute of Experimental Medicine of the Czech Academy of Sciences, 14200 Praha, Czech Republic

Edited by Qi-Qun Tang

Haploinsufficiency of Meis homeobox 2 (*MEIS2*), encoding a transcriptional regulator, is associated with human cleft palate, and *Meis2* inactivation leads to abnormal palate development in mice, implicating MEIS2 functions in palate development. However, its functional mechanisms remain unknown. Here we observed widespread MEIS2 expression in the developing palate in mice. *Wnt1*^{Cre}-mediated *Meis2* inactivation in cranial neural crest cells led to a secondary palate cleft. Importantly, about half of the *Wnt1*^{Cre};*Meis2*$^{f/f}$ mice exhibited a submucous cleft, providing a model for studying palatal bone formation and patterning. Consistent with complete absence of palatal bones, the results from integrative analyses of MEIS2 by ChIP sequencing, RNA-Seq, and an assay for transposase-accessible chromatin sequencing identified key osteogenic genes regulated directly by MEIS2, indicating that it plays a fundamental role in palatal osteogenesis. *De novo* motif analysis uncovered that the MEIS2-bound regions are highly enriched in binding motifs for several key osteogenic transcription factors, particularly short stature homeobox 2 (SHOX2). Comparative ChIP sequencing analyses revealed genome-wide co-occupancy of MEIS2 and SHOX2 in addition to their colocalization in the developing palate and physical interaction, suggesting that SHOX2 and MEIS2 functionally interact. However, although SHOX2 was required for proper palatal bone formation and was a direct downstream target of MEIS2, *Shox2* overexpression failed to rescue the palatal bone defects in a *Meis2*-mutant background. These results, together with the fact that *Meis2* expression is associated with high osteogenic potential and required for chromatin accessibility of osteogenic genes, support a vital function of MEIS2 in setting up a ground state for palatal osteogenesis.

Myeloid ectopic viral integration site (MEIS)[4] transcription factors, the members of the three-amino-acid loop (TALE) superclass, are highly conserved in vertebrates (1). Humans and mice possess three MEIS proteins (MEIS1, MEIS2, and MEIS3) that contain an atypical TALE homeodomain for DNA binding. On a genome-wide scale, the prevailing view is that MEIS proteins act as cofactors for homeobox (HOX) proteins, a subset of homeobox proteins, with or without pre-B cell leukemia transcription factor (PBX) to regulate target gene expression and endow the initially similar segments with their distinct features, except in the first branchial arch (HOX proteins are not expressed in the first branchial arch). MEIS proteins improve the binding affinity and specificity of HOX proteins by directly regulating HOX protein activity. On the other hand, MEIS proteins can also bind DNA independently or cooperatively with other transcription factors (2). Interestingly, studies using mouse models uncovered that MEIS proteins occupy a broad spectrum of common regions involved in the development of entire visceral skeleton in the HOX-negative first branchial arch and HOX-positive second branchial arch, suggesting that MEIS proteins provide a common ground state in all arches (3).

Although all MEIS proteins share a highly similar identity and function redundantly, MEIS1–MEIS3 appear to have distinct functions in embryonic development. *Meis1*-null mice die on embryonic day 14.5 (E14.5) with liver hypoplasia, hemorrhage, and impaired erythropoiesis (4). *Meis3*-null zebrafish show abnormal hind brain formation (5). Although *Meis2*-null mice displayed embryonic lethality between E13.5 and E14.5, with hemorrhage and a small liver size, similar to *Meis1*-null mice, conditional knockout of *Meis2* by *AP2α*^{Cre} in developing neural crest cells results in a defective craniofacial skeleton and abnormal palate (6). Significantly, patients with a *de novo* sequence variant in *MEIS2* or a deletion on chromosome 15q14

This work was supported by Foundation for the National Institutes of Health Grant R01 DE026482 (to Y. C.). The authors declare that they have no conflicts of interest with the contents of this article. The content is solely the responsibility of the authors and does not necessarily represent the official views of the National Institutes of Health.

This article contains Figs. S1–S7, Tables S1–S4, experimental procedures, and references.

[1] Supported by a fellowship from the China Scholarship Council.
[2] Supported by the Czech Science Foundation (18-00514S).

[3] To whom correspondence should be addressed. E-mail: ychen@tulane.edu.

[4] The abbreviations used are: MEIS, myeloid ectopic viral integration site; TALE, three-amino-acid loop extension; HOX, homeobox; PBX, pre-B cell leukemia transcription factor; E14.5, embryonic day 14.5; CNC, cranial neural crest; ChIP-Seq, ChIP sequencing; A-P, anterior-posterior; P0, postnatal day 0; CCP, complete cleft palate; ICP, incomplete cleft palate; FDR, false discovery rate; GO, gene ontology; DEG, differentially expressed gene; TSS, transcription start site; ATAC-Seq, assay for transposase-accessible chromatin with high-throughput sequencing; QC, quality control; crRNA, CRISPR RNA; IP, immunoprecipitation.

affecting *MEIS2* suffered from recurrent features, including cleft palate. The degrees of cleft palate in such patients varies from mild (submucous cleft palate or bifid uvula) to severe (overt cleft lip and palate). Thus, the *MEIS2*-related syndrome was attributed to haploinsufficiency of this gene, indicating that MEIS2 plays an indispensable role in normal palate development (7). However, the detailed role of MEIS2 in palatal development remains known.

Development of the mammalian palate, derived from the HOX-negative first branchial arch, is a highly dynamic process that involves outgrowth, elevation, and fusion of the primary and secondary palate. This complex process is governed by the interactions of multiple signaling pathways and transcription factors. The primary palate originates from embryonic frontonasal prominence and develops into a small part of the adult hard palate anterior to the incisive fossa, whereas the secondary palate arises from paired maxillary processes of the first pharyngeal arch, known as palatal shelves, and consists of the dominating portion of the hard palate and the entire posterior soft palate (8, 9). Although the initial palatal mesenchymal cells are completely derived from the cranial neural crest (CNC), the anterior two-thirds of the palate undergo osteogenesis to form the bony hard palate, which consists of the palatine process of the maxilla and the horizontal plate of the palatine bone. The rest of the palate is also populated by mesoderm-derived muscle progenitors to form muscular soft palate.

Although a growing number of studies have revealed the importance of numerous genes in palate development (10), most of these targeted mutant mouse models exhibit complete cleft of the secondary palate. Submucous cleft palate, also known as incomplete cleft palate, is a rare type of cleft palate, defined as malformed palatal bone and/or abnormal soft palate (11), allowing mechanistic studies of osteogenesis and patterning of the palatal bone during development. Gene inactivation studies imply a critical role of *Bmpr1*a and *Tbx22* in palatal bone formation (12, 13). Our previous studies showed that short stature homeobox 2 (*Shox2*), encoding a paired-like homeodomain transcription factor, is expressed specifically in the anterior palatal mesenchyme, overlapping with the future palatine process of the maxilla (14, 15). *Shox2*-deficient mice exhibit a rare type of incomplete cleft in the anterior palate and defective palatal bone formation (14). SHOX2 ChIP-Seq on the developing limb revealed substantial co-occupation of HOX–TALE factors around skeletogenic genes (16). Furthermore, unbiased *de novo* motif discovery identified high enrichment of MEIS/PBX motifs in genome-wide SHOX2-bound sites in the developing palate, suggesting that SHOX2 acts as transcription partner for TALE proteins in the HOX-negative developing palate (16). However, whether SHOX2 and MEIS/PBX have functional interactions and exhibit genome-wide co-occupancy in the HOX-negative palate remains unknown.

In this study, we showed that MEIS2 is widely expressed in the developing palate and that tissue-specific inactivation of *Meis2* in CNC-derived palatal mesenchyme, but not the palatal epithelium, causes cleft palate, including submucous cleft palate (cleft soft palate) in mice. We subsequently conducted a comprehensive investigation of the functional mechanisms of MEIS2 in palatogenesis at the cellular, molecular, and genomic levels.

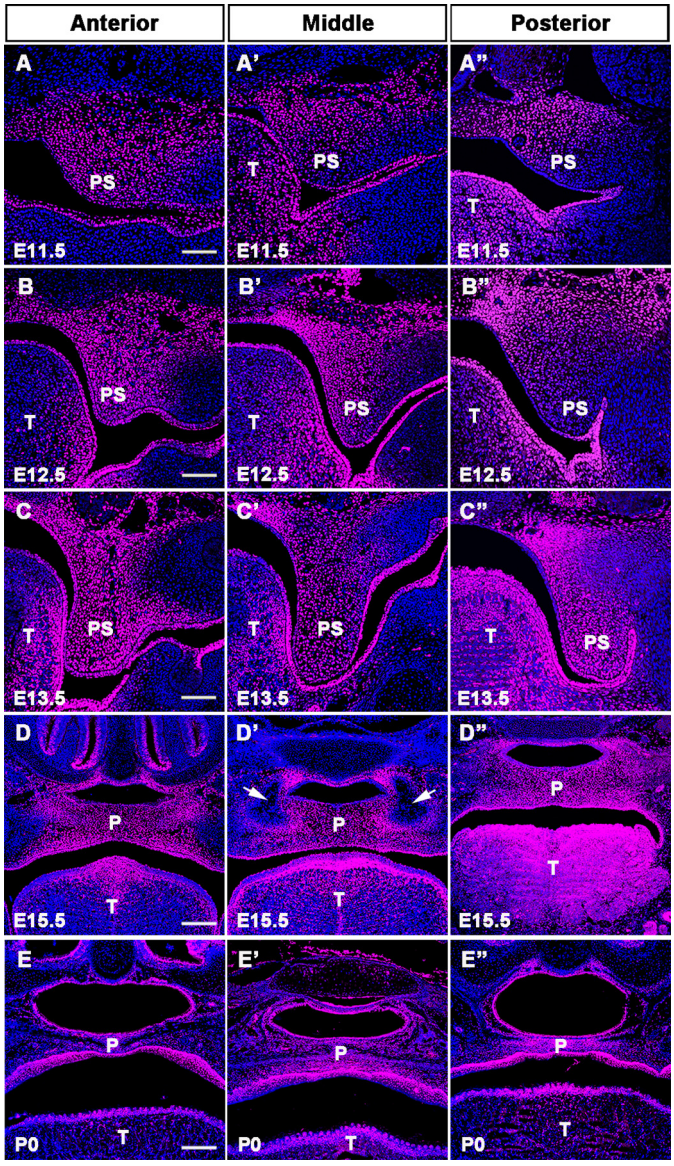

Figure 1. MEIS2 expression in developing palatal shelves. *A–E″*, immunostaining using anti-MEIS2 antibody shows strong expression of MEIS2 in the palatal epithelium and mesenchyme throughout the A-P axis of the developing palate. The section levels indicate the domains along the A-P axis: *Anterior*, the palatine process of the maxilla; *Middle*, the palatine; *Posterior*, the soft palate. Two unique MEIS2-negative domains are located at either end of the nasal passage just dorsal to the palate in *D′* (*white arrows*). *Scale bars* = 100 μm (*A–C″*) and 200 μm (*D–E″*). *T*, tongue; *PS*, palatal shelf; *P*, palate.

Results

Conditional inactivation of Meis2 in CNC cells leads to cleft of the secondary palate

To unmask the role of MEIS2 in palatogenesis, we started with examination of MEIS2 expression by immunostaining in the developing palate. We found that MEIS2 is strongly expressed in the epithelium and mesenchyme along the anterior-posterior (A-P) axis throughout the entire phase of palate development, from E11.5 until postnatal day 0 (P0) (Fig. 1). Additionally, we observed, at the palatine level (defined as the

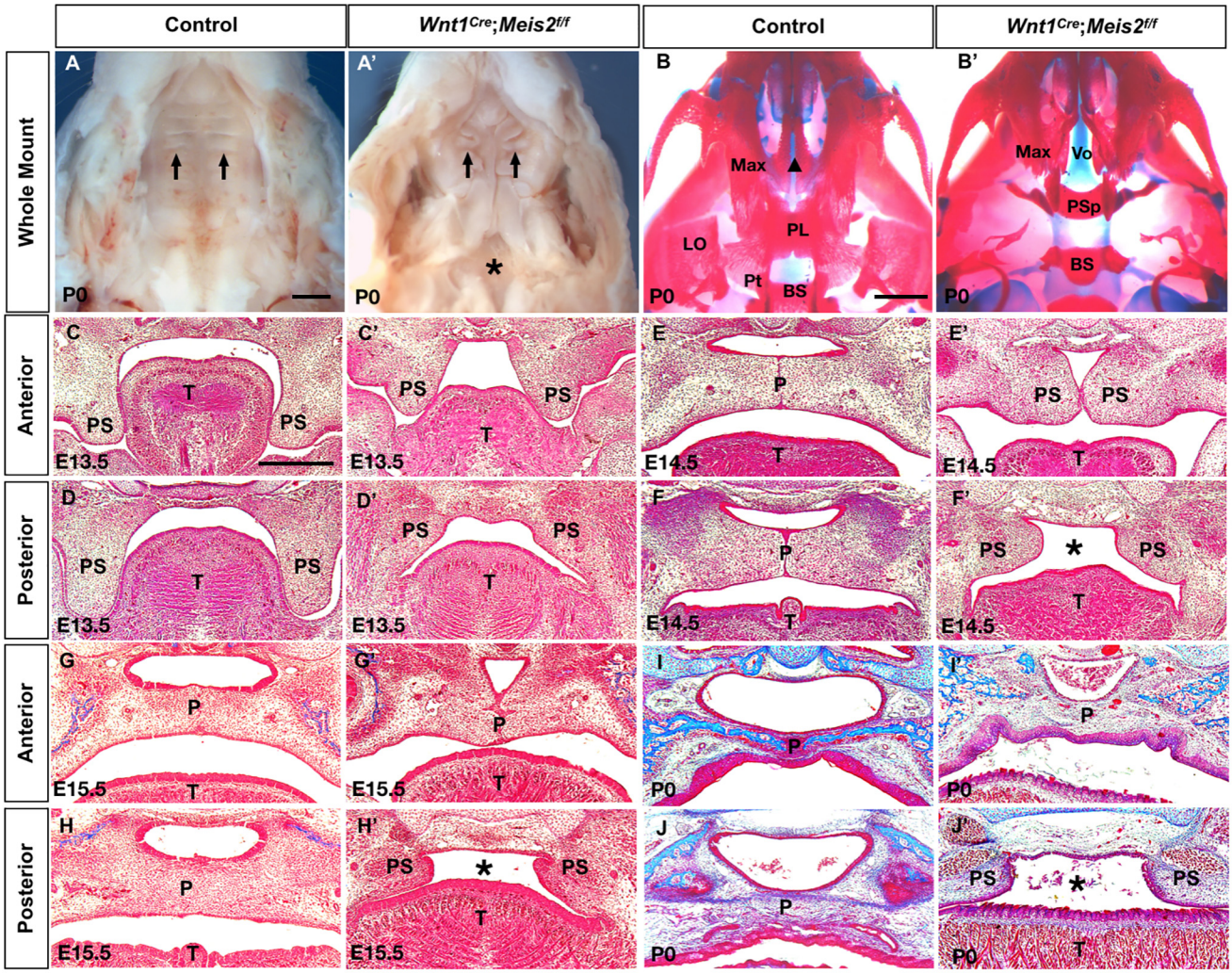

Figure 2. Conditional deletion of *Meis2* in CNC cells leads to submucous cleft. *A* and *A′*, oral view showing disorganized rugae (*black arrows*) and cleft soft palate in *Wnt1*^{Cre};*Meis2*$^{f/f}$ mice at P0 compared with the control. *B* and *B′*, skeletal staining shows complete loss of palatal bones, including the palatine process of the maxilla (*black triangle* in the control) and the palatine bone as well as abnormal lamina obturans and pterygoid in *Wnt1*^{Cre};*Meis2*$^{f/f}$ mice at P0 compared with the control. The vomer and presphenoid in *B′* are not visible in *B* because they are under the maxilla and palatine. *C–J′*, histological examination shows the histology of the developing palatal shelves in WT and *Wnt1*^{Cre};*Meis2*$^{f/f}$ mice from E13.5 to P0. Generally, although the anterior palatal shelves appeared to be slightly malformed in *Wnt1*^{Cre};*Meis2*$^{f/f}$ mice, they elevated, met, and eventually fused in the midline. However, the posterior palatal shelves exhibited dramatically reduced size, never met and failed to fuse, causing cleft soft palate (*asterisks* in *A′*, *H′*, *F′*, *J′*). In addition, mutants also showed a deformed tongue compared with the control. *Scale bars* = 1 mm (*A*--*B′*) and 200 μm (*C–J′*). *T*, tongue; *PS*, palatal shelf; *P*, palate; *Max*, maxilla; *PL*, palatine; *LO*, lamina obturans; *Vo*, vomer; *PSp*, presphenoid; *Pt*, pterygoid; *BS*, basisphenoid.

middle level), two unique MEIS2-negative domains that locate at either end of the nasal passage just dorsal to the palate and eventually become part of maxillary bone (Fig. 1*D′*).

To determine the tissue-specific requirement of MEIS2 in palatal development, we generated *Meis2* conditional mutants by compounding the floxed *Meis2* conditional allele (6) with *K14*^{Cre} or *Wnt1*^{Cre} allele to delete *Meis2* from either palatal epithelium or mesenchyme. Although epithelium-specific inactivation of *Meis2* did not produce any overt phenotype (data not shown), *Meis2* deletion in CNC-derived palatal mesenchyme by *Wnt1*^{Cre} (Fig. S1) indeed led to cleft of the secondary palate, similar to that seen in *AP2α*^{Cre};*Meis2*$^{f/f}$ mice (6). Close gross examination of mutant mice identified two types of cleft palate defects: complete cleft palate (CCP) (47.6%, 81 of 170) and submucous cleft, referred to here as incomplete cleft palate (ICP) (52.4%, 89 of 170), manifested as disorganized palatal rugae and cleft soft palate (Fig. 2, *A* and *A′*, and Fig. S2, *A* and *A′*). Whole-mount skeletal staining of newborn pups showed that all *Meis2* mutants with ICP or CCP displayed complete absence of palatal bones, including the palatine process of the maxilla and palatine bone, as well as loss of lamina obturans and pterygoid (Fig. 2, *B* and *B′*, and Fig. S2, *B* and *B′*). Histological examination of mutant embryos compared with controls revealed that all mutants had smaller palatal shelves in the posterior portion, where the soft palate would form (Fig. 2 and Fig. S2). A BrdU labeling assay confirmed significantly reduced cell proliferation rates in the posterior palatal mesenchyme but not in the anterior palate, in line with a down-regulated expression level of Cyclin D1 and A2 (Fig. S3 and data not shown). Moreover, the comparable levels of caspase 3 in control and mutant palates at E13.5 and E16.5 indicated that *Meis2* deletion does not affect cell apoptosis (data not shown). However, although in some mutants, the anterior portion of the palatal shelf also appeared to be deformed and failed to elevate (Fig. S2 and data

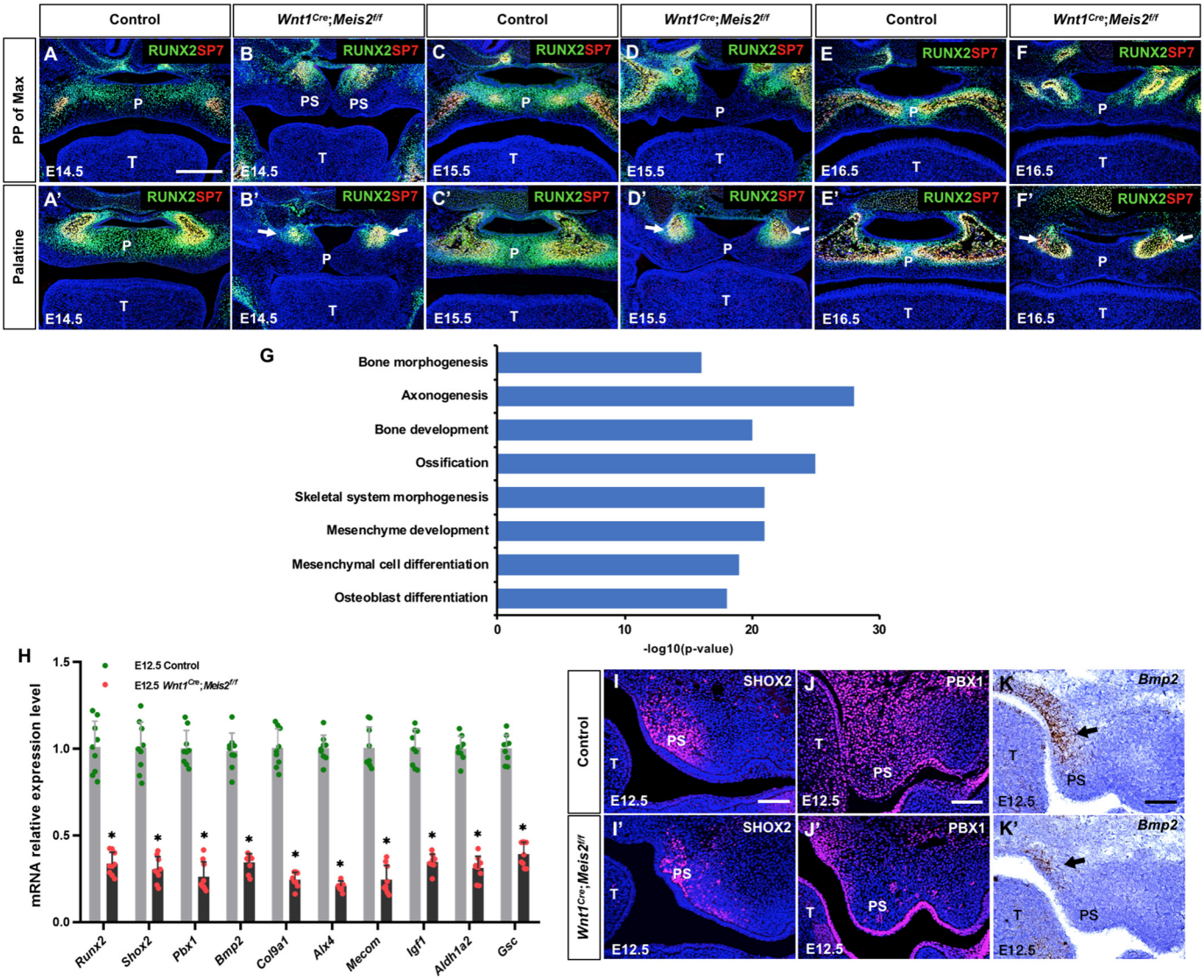

Figure 3. Meis2 inactivation down-regulates expression of osteogenic genes in the developing palate. *A--F′*, immunostaining shows absence of the osteogenic markers RUNX2 and SP7 in the palate of *Wnt1*^{Cre};*Meis2*$^{f/f}$ mice at E14.5–E16.5 compared with the WT. At the either end of the nasal passage just dorsal to the palate, where MEIS2 was not expressed, the expression of RUNX2 and SP7 remained (*white arrows* in *B′*, *D′*, and *F′*). *G*, GO analysis of RNA-Seq results reveals that the down-regulated genes in the palatal mesenchyme of E12.5 *Wnt1*^{Cre};*Meis2*$^{f/f}$ mice are highly associated with osteogenesis. *H*, RT-qPCR analysis validates down-regulation of selected osteogenic genes in E12.5 *Wnt1*^{Cre};*Meis2*$^{f/f}$ mice as compared with controls. *I--K′*, immunostaining and *in situ* hybridization further confirm down-regulation of SHOX2 (*I′*), PBX1 (*J′*), and *Bmp2* (*K′*, *black arrows*) in E12.5 *Wnt1*^{Cre};*Meis2*$^{f/f}$ anterior palatal shelves compared with the control. *Scale bars* = 100 μm (*A–F′* and *I–K′*). *, $p < 0.05$. *PP of Max*, palatine process of the maxilla; *T*, tongue; *PS*, palatal shelf; *P*, palate.

not shown), some mutant embryos exhibited relatively normal anterior palatal shelves that were able to elevate and meet at the midline (Fig. 2, *E′*, *G′*, and *I′*). Histological examination of P0 mutants with ICP further confirmed failed bone formation in the hard palate domain (Fig. 2, *I* and *I′*). Additionally, the tongue of mutant mice appeared to be smaller and exhibited disorganized muscle fibers compared with controls (Fig. S2, *E–F′*).

Deletion of Meis2 down-regulates the expression of osteogenic genes

The complete absence of the palatal bones in *Wnt1*^{Cre};*Meis2*$^{f/f}$ mice indicates an essential role of MEIS2 in osteogenesis during palatogenesis. Because most genetically modified animal models present a complete cleft palate phenotype, *Wnt1*^{Cre};*Meis2*$^{f/f}$ mice with ICP are an excellent model for studying MEIS2's function in palatal osteogenesis *in situ*. We chose mutant embryos whose anterior palatal shelves had elevated at E14.5 and fused at the following stages for detailed analyses. Because palatal bone formation undergoes intramembranous ossification, which requires RUNX2 and SP7, we conducted immunostaining for these two initial bone markers. At E14.5–E16.5, we failed to detect RUNX2 and SP7 expression in the entire future hard palate domain of the mutants (Fig. 3, *A–F′*), indicating failure of initial osteogenesis in the developing palate. Interestingly, the parts of the maxillary bone at the either end of the nasal passage within the palatine domain formed nevertheless, consistent with the lack of MEIS2 expression in these two sites (Figs. 1*D′* and 3, *B′*, *D′*, and *F′*).

To profile MEIS2-regulated gene expression involved in palatal osteogenesis, we performed RNA-Seq in the anterior palatal mesenchyme of *Wnt1*^{Cre};*Meis2*$^{f/f}$ and control mice at stages before osteogenic differentiation (E12.5) and after initiation of

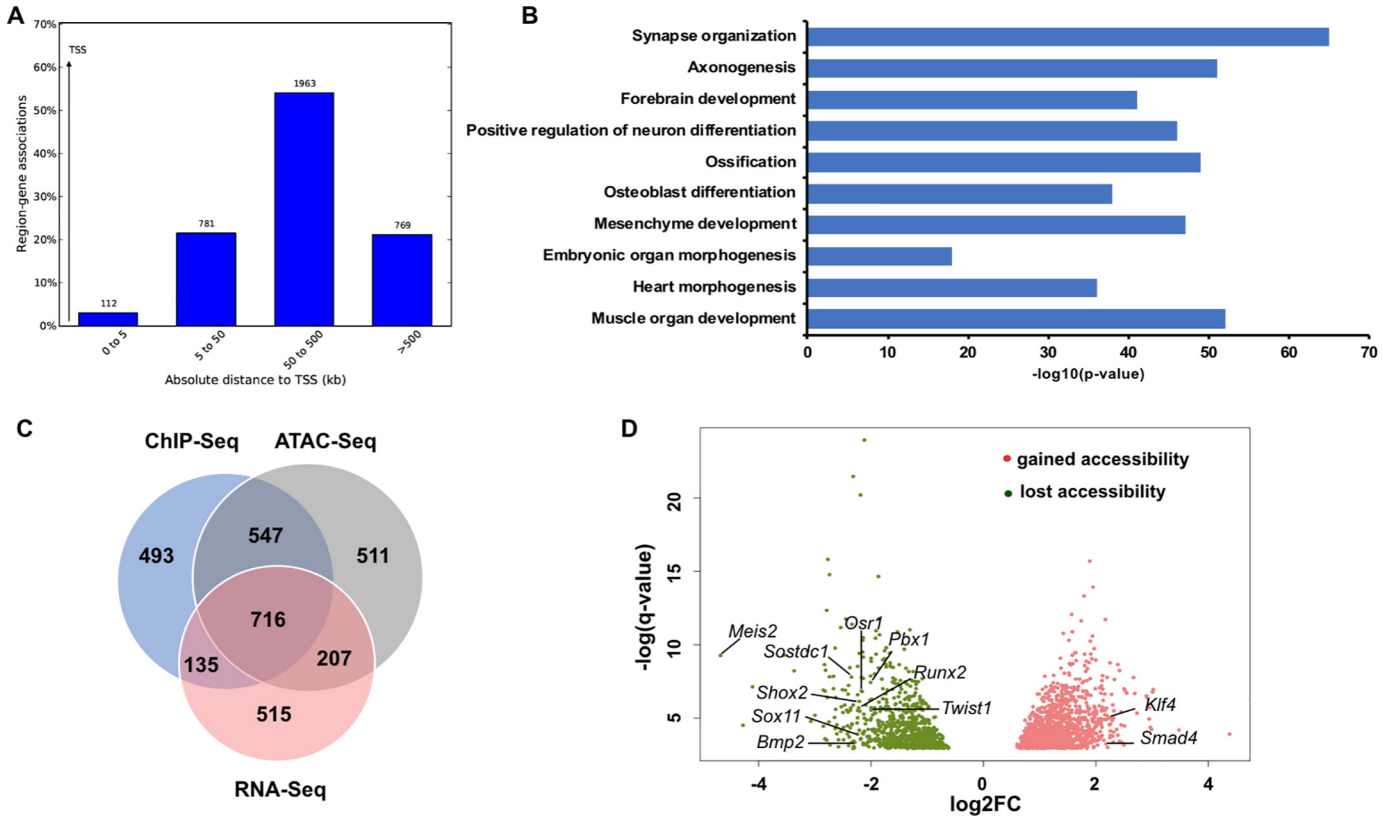

Figure 4. MEIS2 binds to osteogenic gene loci directly and arranges chromatin accessibility. *A*, the majority of MEIS2-bound regions have great distance to its nearest TSS. *B*, GO analysis of MEIS2 ChIP-Seq datasets indicates that genes near MEIS2-bound sites are associated with ossification and osteoblast differentiation. *C*, Venn diagram shows the overlapping genes identified by MEIS2 ChIP-Seq, ATAC-Seq, and RNA-Seq. *D*, volcano plots show the regions that lose chromatin accessibility in E12.5 $Wnt1^{Cre};Meis2^{f/f}$ mice are linked to key osteogenic genes.

osteogenesis (E15.5) with biological triplicates. At E12.5, 1613 genes were responsive to *Meis2* inactivation, with $p < 0.05$ and a false discovery rate (FDR) < 0.05. Among them, 782 genes were expressed at significantly lower levels, and 831 genes were up-regulated in *Meis2* mutants compared with controls (Table S1). Gene ontology (GO) analysis showed that most of the significant terms associated with those down-regulated genes are osteogenesis-related, such as bone morphogenesis, bone development, ossification, and skeletal system morphogenesis (Fig. 3*G*). To validate the RNA-Seq results, we assayed the expression of some selected genes (*Runx2*, *Shox2*, *Pbx1*, *Bmp2*, *Col9a1*, *Alx4*, *Mecom*, *Igf1*, *Aldh1a2*, and *Gsc*) by RT-PCR and confirmed significant down-regulation of these genes in the mutant palatal mesenchyme compared with controls (Fig. 3*H*). Concordantly, immunostaining and *in situ* hybridization assays further verified down-regulation of SHOX2, PBX1, and *Bmp2* expression in the mutant palatal shelves (Fig. 3, *I–K'*). Furthermore, RNA-Seq results of E15.5 palate revealed a total number of 1240 differentially expressed genes (DEGs), including 471 down-regulated and 769 up-regulated ones with $p < 0.05$ and FDR < 0.05. Similarly, these DEGs were also highly related to ossification, biomineral tissue development, bone mineralization, regulation of biomineral tissue development, and bone development (Fig. S4*A*). In addition to down-regulated expression of *Runx2*, *Shox2*, *Pbx1*, and *Bmp2*, RT-qPCR also confirmed dramatically reduced expression of osteogenic differentiation markers, including *Sp7*, *Dmp1*, *Col1a2*, *Spp1*, and *Osr1* (Fig. S4, *B–E'*).

MEIS2 directly binds to osteogenic genes in the palate

To define the direct targets of MEIS2 in the palatal mesenchyme, we generated a $Meis2^{HA}$ knock-in allele that allows effective immunoprecipitation of HA-tagged MEIS2 (Fig. S5*A*). The expression pattern of HA-tagged MEIS2 was confirmed by immunostaining (Fig. S5*B*), and heterozygous and homozygous $Meis2^{HA}$ mice appeared to be normal and fertile, indicating that the HA tag does not disrupt MEIS2's function (data not shown). To match the RNA-Seq results, we conducted MEIS2 ChIP-Seq using an HA antibody on the palatal mesenchyme from E12.5 $Meis2^{HA}$ mice. The majority of the MEIS2-bound peaks have a great distance to its nearest transcription start sites (TSSs; Fig. 4*A*) and were assigned to 1891 coding genes. GO analysis revealed association of these genes to ossification (including *Shox2*, *Runx2*, *Pbx1*, and *Bmp2*), osteoblast development, and embryonic organ morphogenesis (Fig. 4*B* and Table S2).

To further confirm the ChIP-Seq results and to define the chromatin landscape in palatal mesenchymal cells with and without MEIS2, we performed assay for transposase-accessible chromatin sequencing (ATAC-Seq) on palatal cells from E12.5 *Meis2* mutants and controls. Quality control (QC) analysis indicated that all ATAC-Seq libraries possessed the expected fragment size distribution, with a large proportion of fragments less than 100 bp, representing nucleosome-free regions (Fig. S5*C*). In controls, 85.83% of reads were mapped to mm10 reference genomes, and about 140,000 regions of accessible chromatin were identified. On the other hand, 88.85% of reads were

mapped, and about 120,000 regions were identified in the *Meis2* mutant group. Comparison of the distribution of genomic annotation between controls and mutants showed that most ATAC-Seq peaks were mapped to regions within several hundred base pairs of TSSs but exhibited a prominent difference in the percentage of the promoters, introns, and intergenic regions in the mutants compared with controls. These results demonstrate that the chromatin accessibility of the promoters and enhancers is affected by deletion of *Meis2* (Fig. S5, *D* and *E*). To establish the correlation between chromatin accessibility and transcriptional regulation, we annotated the MEIS2-related open chromatin regions to the nearest genes, with $p < 0.05$ and FDR < 0.05 (Table S3). In the absence of *Meis2*, 1067 chromatin regions annotated to 761 genes lost their accessibility, whereas 1721 chromatin regions annotated to 1211 genes gained the accessibility. We subsequently conducted integrative analyses of the ATAC-Seq, RNA-Seq, and MEIS2 ChIP-Seq datasets. As expected, hundreds of genes linked to MEIS2-related open chromatin regions were occupied by MEIS2 and showed a transcriptional change (Fig. 4*C*). The key osteogenic genes bound by MEIS2, including *Runx2*, *Shox2*, *Pbx1*, *Bmp2*, *Osr1*, and *Twist1*, were down-regulated at the transcriptional level with $p < 0.01$ and FDR < 0.01 (Table S1) and lost their chromatin accessibility, including the coding regions and MEIS2-bound distal regulatory regions (Figs. 4*D* and Fig. 5*D*). These results indicate that MEIS2 binds directly to the osteogenic genes loci, arranges chromatin accessibility, and eventually regulates transcriptional profiles during palatal osteogenesis.

Cooperation of MEIS2 and SHOX2 during palatal osteogenesis

To identify potential transcription factors that also bind to the MEIS2-bound regions, we performed *de novo* motif analysis on the binding peaks of MEIS2 in the palate (Fig. 5*A*). In addition to factors involved in neural crest development, such as FOXC2 and HOXA10, the MEIS2-bound regions were enriched for binding motifs of transcription factors involved in bone formation, including SHOX2, RUNX2, PBX1, and ASCL2.

We have reported previously that TALE-related motifs are enriched in SHOX2-bound peaks in the palate (16), consistent with enrichment of SHOX2-bound motifs in MEIS2-bound regions. We have demonstrated that most of the SHOX2-bound regions are likely distal regulatory elements, as demonstrated by the enhancer activity of several selected SHOX2-bound DNA fragments in transient transgenic reporter assays (15, 16). Together, these results suggest that SHOX2 and MEIS2 function as partners to regulate gene expression and palatal osteogenesis. To test this hypothesis, we performed double immunostaining and found extensive but not complete colocalization of MEIS2 and SHOX2 in the palatal mesenchyme (Fig. S6, *A–B'*). A coimmunoprecipitation assay of culture cells and a Duolink proximity ligation assay on palatal mesenchymal cells were performed as described in the supporting experimental procedure, and confirmed the physical interaction between MEIS2 and SHOX2 (Fig. S6, *C–D'*). We subsequently intersected our MEIS2 ChIP-Seq datasets with our published SHOX2 ChIP-Seq results on the E12.5 anterior palate (16). Indeed, the majority of MEIS2-bound regions were also occupied by SHOX2, indicating genome-wide co-occupancy of SHOX2 and MEIS2 (Fig. 5*B*). Furthermore, functional annotation of MEIS2 ChIP-Seq and SHOX2 ChIP-Seq datasets identified almost the same GO terms, such as embryonic organ development, ossification, osteoblast differentiation, and mesenchyme development (Fig. 5*C*). Considering the vital role of MEIS2 and SHOX2 in palatal osteogenesis, we focused on genes from the ossification term that were cobound by MEIS2 and SHOX2 for further analysis of their chromatin landscape revealed by ATAC-Seq. As shown in Fig. 5*D*, the top osteogenic genes *Shox2*, *Runx2*, *Pbx1*, and *Bmp2* were found to lose accessibility in the *Meis2* mutant palate. Integration of our ChIP-Seq and ATAC-Seq data with the published H3K27ac ChIP-Seq data on the embryonic facial region (17) showed high enrichment of H3K27ac in these regions, indicating active enhancer characteristics of these SHOX2 and MEIS2 cobound regions.

MEIS2 provides the ground state for palatal osteogenesis

Given the dramatic down-regulation of SHOX2 and inaccessibility of the regulatory and coding regions of *Shox2* in the *Meis2* mutant palate and the important role of SHOX2 in palatal bone formation (15, 18), we hypothesized that, as a downstream target of MEIS2, SHOX2 may mediate MEIS2's function in regulating palatal osteogenesis. To test this hypothesis, we overexpressed *Shox2* in CNC cells in the *Meis2* mutant background by compounding the $R26R^{Shox2}$ knock-in allele (19) with $Wnt1^{Cre}$ and $Meis2^{f/f}$ alleles. All $Wnt1^{Cre}$;$Meis2^{f/f}$;$R26R^{Shox2}$ mice ($n = 14$) died soon after birth with ICP (5 of 14, 35.7%) or CCP (9 of 14, 64.3%). The ICP mice likewise manifested a fused anterior palate and cleft soft palate (Fig. S7, *A* and *A'*). Similar to $Wnt1^{Cre}$;$Meis2^{f/f}$ mice, whole-mount skeletal staining of $Wnt1^{Cre}$;$Meis2^{f/f}$;$R26R^{Shox2}$ ICP mice revealed complete loss of the palatal bones (Fig. S7, *B* and *B'*). Immunostaining confirmed lack of RUNX2 expression in the mutant hard palate compared with controls at E16.5 (Fig. S7, *C–D'*). Thus, *Shox2* overexpression failed to rescue the defect of palatal bones in the absence of *Meis2*.

We have reported previously that palatal mesenchymal cells expressing *Shox2* are divided into two subpopulations: one differentiating to osteoblasts and one becoming fibroblasts (15). The observation that SHOX2 and MEIS2 expression overlaps largely but not completely in the palatal mesenchyme (Fig. S6) prompted us to ask whether *Shox2*-positive palatal mesenchymal cells with or without *Meis2* expression possess distinct osteogenic potential. To address this question, we carried out single-cell RNA-Seq on total *Shox2*-expressing palatal mesenchymal cells. We took advantage of existing $Shox2^{Cre}$ knock-in allele and $R26R^{mTmG}$ reporter mice to isolate $Shox2^{+}$ cells by cell sorting. A total number of 3979 GFP-positive cells from E13.5 $Shox2^{Cre/+}$;$R26R^{mTmG}$ palatal mesenchyme were sequenced, and 2953 cells were selected for the subsequent analysis based on QC metrics. After normalization and dimensionality determination, the cells were automatically clustered into five clusters (C0–C4) using Seurat v3. Interestingly, using FeaturePlot, cells in cluster 2 were found to express a remarkably lower level of *Meis2* compared with other clusters (Fig. 6*A*). Using FindMarkers, we identified 455 DEGs between cluster 2 and other clusters with $p < 0.05$ and FDR < 0.05, including 195 genes at lower levels and 260 genes at higher levels in cluster 2

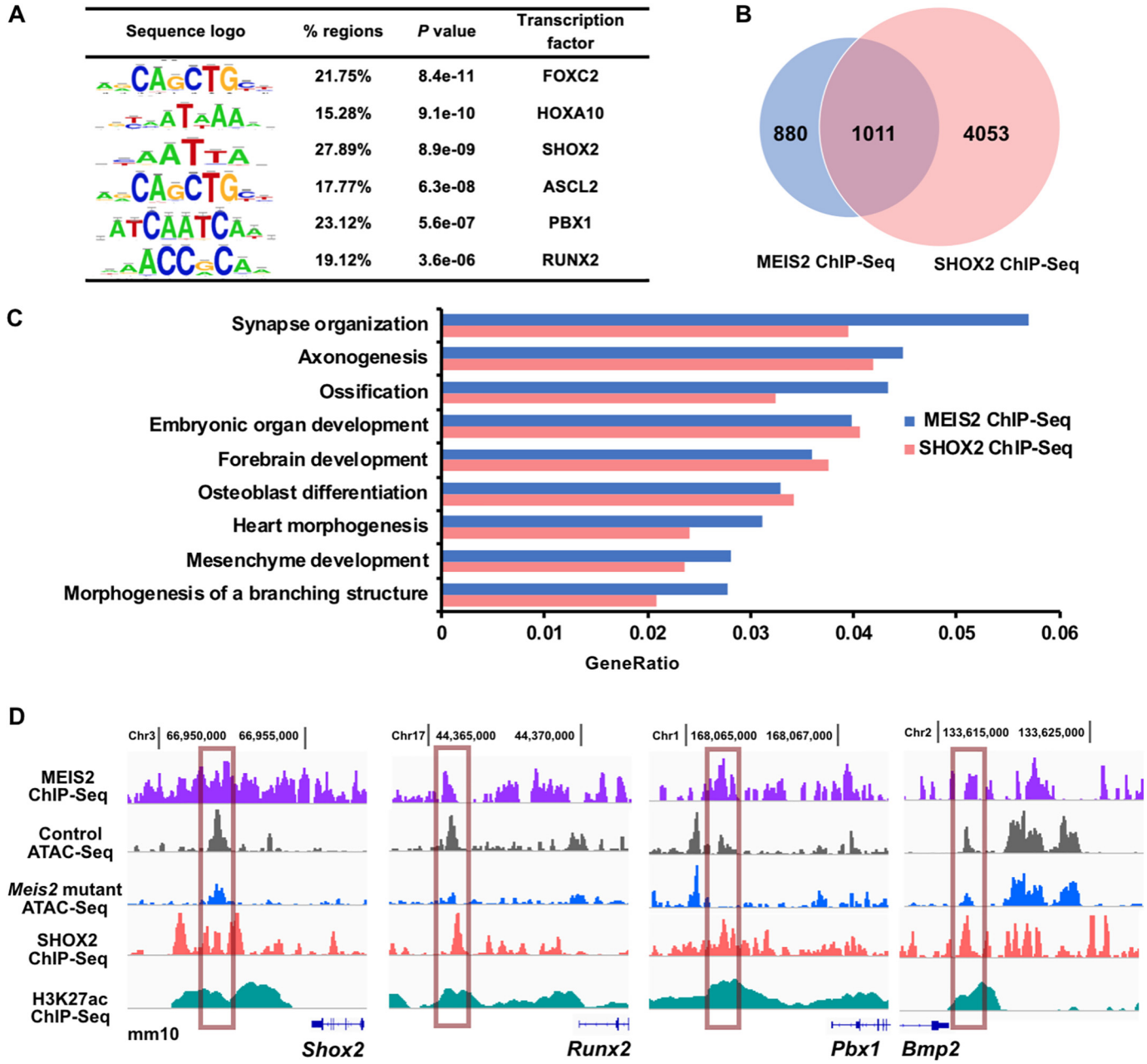

Figure 5. MEIS2 and SHOX2 exhibit co-occupancy on osteogenic gene loci in the palate. *A*, *de novo* motif analysis unravels highly enriched binding motifs of osteogenic factors, including SHOX2, RUNX2, and PBX1 in the MEIS2-bound regions. *B*, a Venn diagram shows extensively overlapped genes bound by MEIS2 and SHOX2 ChIP-Seq to the E12.5 anterior palatal mesenchyme. *C*, a GO analysis reveals the same functional categories of the MEIS2-bound sites (*blue bars*) and SHOX2-bound sites (*red bars*). The *x* axis values correspond to the gene ratio of each term. *D*, MEIS2 directly binds to the distal regions near the *Shox2*, *Runx2*, *Pbx1*, and *Bmp2* loci, which are also occupied by SHOX2 and are enriched in H3K27ac (*boxes*). ATAC-Seq analysis further reveals dramatically reduced chromatin accessibility within these regions in the E12.5 $Wnt1^{Cre}$; $Meis2^{f/f}$ palate.

cells. GO analysis revealed that the genes with lower expression levels are associated with roof of mouth development, regulation of ossification, and ossification (Fig. 6*B*). Indeed, an expression heatmap manifested significantly low expression levels of osteogenic genes in cluster 2 cells (Fig. 6*C*). By comparison with the RNA-Seq data from the E12.5 $Wnt1^{Cre}$;$Meis2^{f/f}$ palate, we found that, among the 22 ossification-associated genes with lower expression levels in *Meis2*-negative cells, 13 were also down-regulated in the mutant palate (Fig. 6*D*). The results suggest that the osteogenic potential of *Shox2*-positive cells is *Meis2*-dependent during palatal osteogenesis. *Meis2* appears to be a key determinant in directing the osteogenic fate of *Shox2*-positive palatal cells. Together with the fact that the key osteogenic genes bound by MEIS2 lost their chromatin accessibility in the absence of *Meis2*, these results pinpoint a fundamental role of MEIS2 in palatal bone formation by setting up a ground state for palatal osteogenesis.

Discussion

In humans, substantial lines of evidence support that *MEIS2* is a candidate gene for cleft palate (7, 20–22), but the mechanisms underlying *MEIS2*-mediated defects are completely

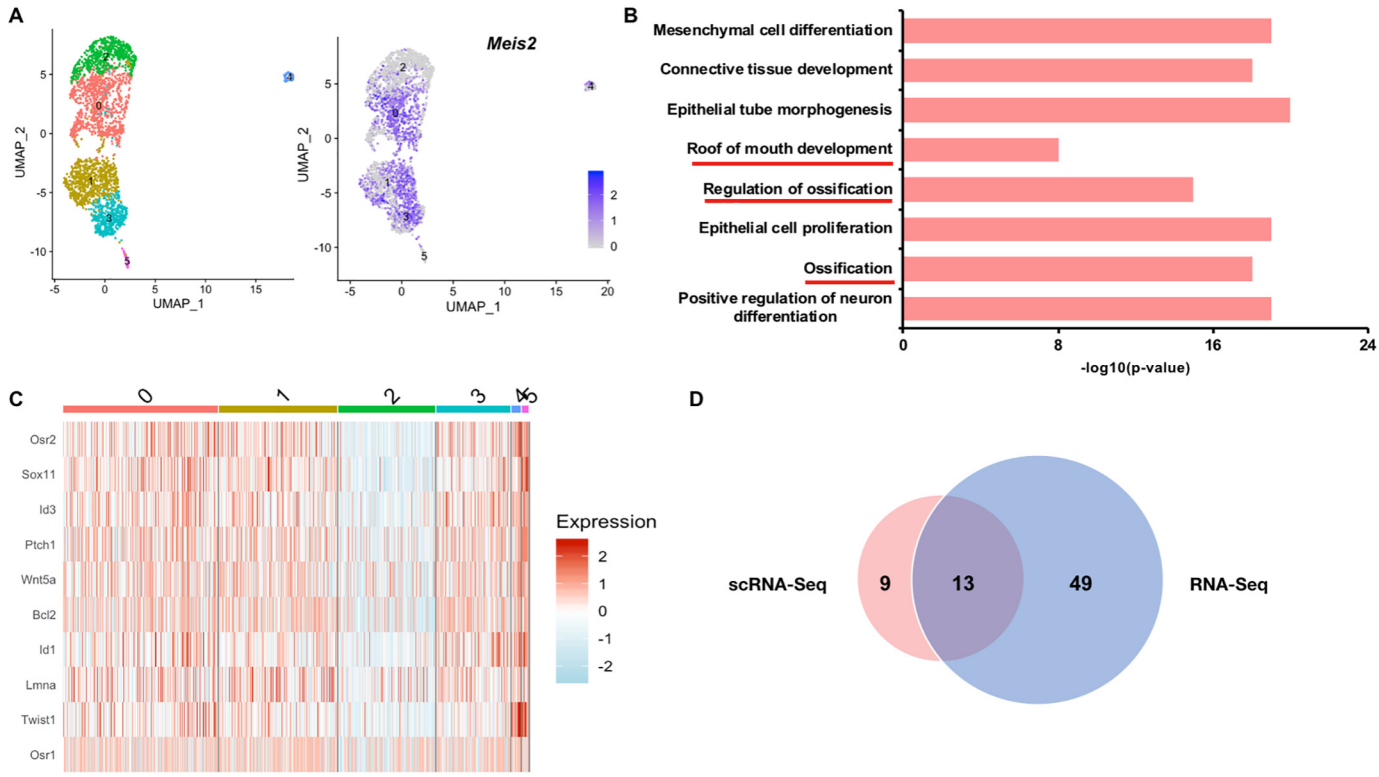

Figure 6. Meis2 is closely associated with osteogenic potential of *Shox2*-expressing cells in developing palatal shelves. *A*, single-cell RNA-Seq analysis shows that E13.5 *Shox2*-positive palatal mesenchymal cells are clustered into five groups, with cluster 2 cells expressing lowest level of *Meis2* (defined as *Meis2*-negative cells) compared with other clusters. *B*, GO analysis reveals that genes with low expression levels in cluster 2 are associated with roof of mouth development, regulation of ossification, and ossification. *C*, expression heatmap confirms the significantly low expression levels of osteogenic genes in cluster 2 (*Meis2*-negative cells). *D*, a Venn diagram shows that more than half of the ossification-associated genes with lower expression levels in cluster 2 are also down-regulated in *Wnt1*^{Cre};*Meis2*$^{f/f}$ palatal shelves.

unknown. In this study, we conducted a comprehensive investigation of the role of MEIS2 in palatal development. Tissue-specific inactivation of *Meis2* in CNC cells led to complete cleft palate or submucous cleft with complete loss of palatal bones. Molecular and genomic analyses demonstrate direct regulation of key osteogenic genes by MEIS2. In addition, we also showed, that in the HOX-negative first branchial arch–derived palate, MEIS2 may act together with SHOX2 to regulate the expression of osteogenic genes by binding to distal regulatory elements. The fact that *Meis2* is highly associated with osteogenic potential and required for chromatin accessibility of osteogenic genes supports a vital function of MEIS2 in providing a ground state for palatal osteogenesis.

Similar to the relatively stabilized but varying features of cleft palate defects in humans with *MEIS2* haploinsufficiency, *Meis2* mutant mice exhibited a typical CCP or ICP, indicating a conserved role of MEIS2 in regulating palatogenesis. Importantly, *Meis2* mutant mice with ICP lack all palatal bones, in contrast to several previously reported animal models with submucous cleft that presented partial defects of palatal bones (12, 13, 23). Although a critical role of MEIS2 in embryonic skeleton development has been reported previously (3, 6), the functional mechanisms of MEIS2 in osteogenesis remain elusive. In this study, we showed that *Meis2* mutant palatal shelves failed to express osteogenic markers, indicating that palatal mesenchymal cells lacking *Meis2* lose their osteogenic fate. These results raise the intriguing possibility that MEIS2 functions in cell fate determination during palatal development. Palatal bones, including the palatine process of the maxilla and the palatine bone, are formed through intramembranous ossification, a process that requires expression of RUNX2 (24). Many other genes have also been implicated in skeleton formation in the craniofacial region, including the palate (18, 25–28). All of these osteogenic genes, including *Runx2*, *Shox2*, *Pbx1*, *Bmp2*, *Twist1*, and *Aldh1a2*, were dramatically down-regulated in the palatal mesenchyme lacking *Meis2*, indicating that MEIS2 functions upstream of a spectrum of osteogenic genes. Intersection of RNA-Seq with MEIS2 ChIP-Seq and ATAC-Seq datasets on the palatal shelves confirmed direct targets of these osteogenic genes by MEIS2. These results demonstrate that MEIS2 functions to establish osteogenic cell fate in palatal mesenchymal cells by directly activating the expression of osteogenic genes. Given the fact that the distal regulatory regions of osteogenic genes that were bound by MEIS2 became inaccessible along with their coding regions, MEIS2 may also acts as an epigenetic modifying factor required for chromatin poising or opening. This is in agreement with previous reports showing that TALE proteins, including PBX and MEIS, have an early role in poising target gene loci for gene activation by HOX proteins (29, 30). It appears that this unique role of TALE proteins as transcription factors is conserved in HOX-negative domains.

In the MEIS2-bound regions, the highly enriched SHOX2, PBX1, and RUNX2 binding motifs implicate that these proteins

act as cofactors for MEIS2 to activate transcription of downstream genes. Indeed, TALE proteins have been shown to act as a functional unit with or without additional transcription factors in all species tested to date (2, 31). Interestingly, these transcription factors were also prominently down-regulated in the absence of *Meis2*, suggesting a complicated regulatory network between MEIS2 and these osteogenic factors in palate development. Among these factors, SHOX2 appears to be a critical cofactor for MEIS2 in palatal bone formation and patterning. This is because *Shox2* is expressed in the hard palate, and its inactivation leads to anterior cleft of the secondary palate with defective palatal bone (15, 18), and MEIS/PBX binding motifs are highly enriched in the SHOX2-bound regions unraveled by SHOX2 ChIP-Seq on the palate (16). As expected, integration of MEIS2 ChIP-Seq and SHOX2 ChIP-Seq datasets on the palate revealed extensive genome-wide co-occupancy of these two factors, suggesting that, in the HOX-negative palate, SHOX2 and TALE proteins act together to regulate gene expression. In the developing palate, these two factors appear to primarily regulate osteogenesis, as both of them bind to distal regulatory elements of osteogenic genes. Although SHOX2 is a downstream target of MEIS2, they appear to function in parallel, as *Shox2* overexpression failed to rescue the bone defects in the palate lacking *Meis2*.

We have reported previously that, although the *Shox2* expression domain is restricted within the anterior hard palate, only a subpopulation of *Shox2*-expressing palatal mesenchymal cells differentiates into osteoblasts, with a subpopulation of *Shox2*-expressing cells eventually becoming fibroblasts (15). Interestingly, although MEIS2 is widely expressed in developing palatal shelves, a closer look identified partial overlap of MEIS2 and SHOX2 in the palatal mesenchyme. Despite the lack of direct evidence showing that *Shox2*-positive cells lacking *Meis2* have a fibroblast fate, unbiased single-cell RNA-Seq analysis revealed a high osteogenic potential of palatal cells expressing *Shox2* and *Meis2* compared with *Shox2*-positive cells without *Meis2* expression. These results indicate a positive role of *Meis2* in the osteogenic trajectory. Taken together with the fact that MEIS2 is required for proper chromatin poising/opening of osteogenic genes, our results support a role of MEIS2 in setting up the ground state for palatal bone formation and patterning.

Experimental procedures

Mouse strains

Generation and genotyping of $Wnt1^{Cre}$, $Meis2^{f/f}$, $R26R^{mTmG}$, $Shox2^{Cre}$, $R26R^{Shox2}$ and $Shox2^{HA}$ alleles have been described previously (6, 19, 32–35). The $Meis2^{HA}$ allele was generated by using the Alt-R CRISPR-Cas9 crRNA kit (Integrated DNA Technologies), following the manufacturer's protocol. Briefly, crRNA was designed to target the 5′ATG of *Meis2* (RRID: SCR_015723). The synthetic crRNAs were duplexed with trans-activating crRNA (tracrRNA) to form single guide RNA. The single guide RNA and Alt-R S.p. Cas9 nuclease were mixed to generate a ribonucleoprotein complex, which was then immediately electroporated into the C57BL/6J zygotes together with the donor DNA, a single-strand oligo DNA nucleotide containing a 2× HA sequence. Viable electroporated embryos at the two-cell stage were transferred to pseudopregnant females to create founders. Two positive male founders were obtained and backcrossed with C57BL/6J females to generate F1 mice. The primers for genotyping of $Meis2^{HA}$ alleles were 5′-CGTTTTCTTGACTGGGCTTTCC-3′ (forward) and 5′-CGCCATCATCATCAAGCAACC-3′ (reverse), which amplified a 348-bp product from the HA tag allele and a 291-bp product from the WT allele. All experiments involving animals in this study were approved by the Institutional Animal Care and Use Committee of Tulane University.

Embryo collection, histological examination, immunostaining, in situ hybridization, and skeletal staining

Embryos with *Meis2* inactivation in CNC cells ($Wnt1^{Cre}$; $Meis2^{f/f}$) were generated by compounding $Meis2^{f/f}$ mice with $Wnt1^{Cre}$ line, and embryos with *Shox2* overexpression in the absence of *Meis2* were obtained by combining $R26R^{Shox2}$, $Wnt1^{Cre}$, and $Meis2^{f/f}$ alleles. All embryos were harvested from euthanized timed pregnant females. For skeletal staining and immunostaining, heads from embryos or newborn pups were fixed in 4% paraformaldehyde in PBS at 4 °C overnight, decalcified (only for newborn pups), dehydrated through graded ethanol, embedded in paraffin, and sectioned at 8 μm. A cell proliferation assay was performed by BrdU injection 2 h prior to sample harvest. The primary antibodies for immunostaining were as following: anti-MEIS2 (Abcam, ab73164, 1:200), anti-RUNX2 (Santa Cruz, sc-390351, 1:300), anti-SP7 (Abcam, ab22552, 1:300), anti-BrdU (Novus Biologicals, NB100-1614, 1:300), anti-Cyclin A2 (Abcam, ab32386, 1:300), anti-Cyclin D1 (Abcam, ab16663, 1:300), anti-caspase 3 (Cell Signaling Technology, 9661, 1:300), anti-HA (Genscript, A00168-40, 1:300), anti-SHOX2 (homemade, 1:250), anti-PBX1 (Cell Signaling Technology, 4342S, 1:250), and anti-MF20 (Developmental Studies Hybridoma Bank, 1:50). The secondary antibodies, purchased from Life Technologies, included donkey anti-rabbit, donkey anti-mouse, donkey anti-goat, and donkey anti-chicken; all were used at 1:1000 dilution. For *in situ* hybridization, embryos were fixed overnight in 10% paraformaldehyde at room temperature, dehydrated with graded ethanol, paraffin-embedded, and sectioned at 5 μm. *In situ* hybridization was carried out with RNAscope Probe-Mm-*Bmp2* (Advanced Cell Diagnostics, 406661) and RNAscope 2.5 HD Assay Brown (Advanced Cell Diagnostics), as described previously (36). Skeletal staining of mouse heads was performed using Alcian blue (for cartilage) and Alizarin Red S (for bone), as described previously (37).

RNA isolation, sequencing, data analysis, and quantitative RT-PCR (RT-qPCR) analyses

For the bulk RNA-Seq assay, the anterior palatal mesenchyme from E12.5 and E15.5 $Wnt1^{Cre}$;$Meis2^{f/f}$ and WT embryos was collected after removal of the palatal epithelium using Dispase II (Sigma). Three biological replicates from each group and genotype were collected for analyses. Total RNA was isolated using the RNeasy Micro Plus Kit (Qiagen). Reverse transcription and amplification of RNA were done and followed by library preparation with the TruSeq RNA

Sample Preparation Kit v2 (Illumina). Subsequently, single-end high-output flow cell sequencing was performed on an Illumina NexSeq 500. Sequencing reads were mapped to a reference mouse genome (GRCm38/mm10) with HISAT2 (default parameters) (38). Gene expression was counted using featureCounts (39), and the DEGs were further processed with DESeq2 (40). Genes with a $\log_2$-fold change (FC) of −1 or less were termed "down-regulated genes," and those with a $\log_2$-fold change of +1 or more were defined as "up-regulated genes". GO analysis was performed using the clusterProfiler R package (41).

For RT-qPCR, RNA from embryonic palatal mesenchyme was reverse-transcribed into complementary DNA using the RevertAid First Strand cDNA Synthesis Kit (Thermo Scientific). Quantitative PCR was performed with iTaq Universal SYBR Green Supermix (Bio-Rad) using a 7500 Fast Real-Time PCR System (Applied Biosystems). The primer sequences are listed in Table S4. Cycle threshold (Ct) values were normalized to *Gapdh*, and the fold changes were calculated according to the $2^{-\Delta Ct}$ method. Student's *t* test was applied to determine the significance of statistical differences between two groups, and results were presented as mean ± S.D. $p < 0.05$ was perceived as statistical significance.

ChIP, library preparation, sequencing, and data analysis

The anterior palate mesenchyme from E12.5 $Meis2^{HA}$ mouse embryos was fixed in 1% formaldehyde for 10 min and quenched with glycine for 5 min at room temperature. After washing with ice-cold PBS containing protease inhibitor mixture, tissues were dispersed into single-cell suspension on ice. The following ChIP assays were performed with Pierce™ Magnetic ChIP Kit (Thermo Scientific) according to the manufacturer's instructions. Briefly, cells were pelleted in PBS and then resuspended in membrane extraction buffer to isolate nuclei. Purified nuclei were subsequently equilibrated in micrococcal nuclease digestion buffer. Micrococcal nuclease was then added to the nucleus suspension to fragmentize chromatin into one to five nucleosomes (150–900 bp). Immunoprecipitation was performed with a rabbit antibody against mouse HA overnight at 4 °C, followed by 2-h incubation with ChIP-grade protein A/G magnetic beads. After washing, the beads were resuspended with IP elution buffer containing 5 M NaCl and 20 mg/ml proteinase K, and then all of the immunoprecipitate and 10% total input in IP elution buffer were incubated at 65 °C for 1.5 h. DNA was purified using a DNA Clean-Up Column, and sequencing libraries were prepared subsequently using the ChIP-Seq DNA Library Prep Kit for Illumina (Cell Signaling Technology). Paired end 2 × 150-bp reads were gained using Illumina HiSeq 2000 and aligned to the mouse genome mm10 with Bowtie2. After filtration, the bigwig file of ChIP was obtained using bamCompare through normalization to input. Peaks were called with MACS2 callpeak controlled to input. The ChIPseeker R package was used to annotate and visualize peaks, followed by GO analysis with clusterProfiler and *de novo* motif analysis with DREME.

FACS, ATAC-Seq library preparation, sequencing, and data analysis

The GFP-positive anterior palatal shelves were isolated from E12.5 $Wnt1^{Cre};Meis2^{f/+};R26R^{mTmG}$ and $Wnt1^{Cre};Meis2^{f/f};R26R^{mTmG}$ embryos. Samples were subjected to digestion with a mixture of 0.02% collagenase I, II, and IV in Hank's Balanced Salt Solution for 30 min, followed by Accutase solution (Sigma) treatment for 5 min at 37 °C. After stopping the digestion with culture medium containing 10% FBS, cells were washed with PBS containing 3% FBS and then filtered through a 70-μm filter. Suspended cells were sorted by FACS on a BD FACSAria Fusion cell sorter (BD Biosciences). Around 50,000 single GFP-positive cells from each group were obtained and promptly subjected to generation of an ATAC-Seq library, as described previously (42). Libraries were pooled equimolarly and sequenced using a paired-end 75-bp read mid-output kit on an Illumina NexSeq 500 platform. Three biological replicates were implemented for each group. After removal of the adaptor sequences, truncated reads were mapped to mm10 reference genomes with bowtie 2 (43). The bamCoverage was used to generate a bigwig file, which is visible on the Integrative Genomics Viewer (44). Peaks from each group were identified on a pool of triplicates using MACS2 callpeak (45). DiffBind was used to identify sites that exhibited differential accessibility between control and *Meis2* mutant groups (46). ChIPseeker R package was used to annotate ATAC-Seq peaks to identify genes regulated by MEIS2. By comparison with control group, peaks with a -fold change of −1 or less were considered as "lost accessibility," and those with a-fold change of +1 or more were regarded as "gained accessibility." The clusterProfile R package was used to perform the GO analysis.

Single cell RNA-Seq and data analysis

GFP-positive cells from the E13.5 $Shox2^{Cre/+};R26R^{mTmG}$ anterior palatal shelves were collected after cell suspension and purified by FACS. Immediately, about 5000 live cells were loaded onto the 10× Genomics Chromium system, and the library was prepared using the Single-Cell 3′ Library and Gel Bead Kit v3, following the manufacturer's protocol. Sequencing was performed on an Illumina NextSeq 500, and Illumina base-call files (*.bcl) were gained for each sample. After conversion to FASTQ, the files were aligned to mouse genome mm10 with CellRanger 3.1.0. The Seurat 3.0 R package was used for QC and visualization, followed by GO analysis with clusterProfiler.

Data availability

All of the RNA-Seq, ChIP-Seq, ATAC-Seq, and single-cell RNA-Seq data were deposited into the GEO with SuperSeries accession number GSE143914. The rest of data are contained within the manuscript.

Author contributions—L. W., Q. T., and H. L. data curation; L. W., Q. T., and H. L. formal analysis; L. W. and L. L. investigation; L. W. visualization; L. W., Q. T., J. X., and T. Y. methodology; L. W. writing-original draft; Q. T. and T. Y. validation; J. X., T. H., and Y. C. conceptualization; O. M. resources; T. H. and Y. C. supervision; T. H. and Y. C. writing-review and editing; Y. C. project administration.

Acknowledgments—We thank all members of our laboratories for helpful discussions of this study and critical reading of the manuscript.

References

1. Longobardi, E., Penkov, D., Mateos, D., De Florian, G., Torres, M., and Blasi, F. (2014) Biochemistry of the tale transcription factors PREP, MEIS, and PBX in vertebrates. *Dev. Dyn.* **243,** 59–75 CrossRef Medline
2. Schulte, D., and Geerts, D. (2019) MEIS transcription factors in development and disease. *Development* **146,** dev174706 CrossRef Medline
3. Amin, S., Donaldson, I. J., Zannino, D. A., Hensman, J., Rattray, M., Losa, M., Spitz, F., Ladam, F., Sagerström, C., and Bobola, N. (2015) Hoxa2 selectively enhances Meis binding to change a branchial arch ground state. *Dev. Cell* **32,** 265–277 CrossRef Medline
4. Azcoitia, V., Aracil, M., Martínez-A, C., Torres, M. (2005) The homeodomain protein Meis1 is essential for definitive hematopoiesis and vascular patterning in the mouse embryo. *Dev. Biol.* **280,** 307–320 CrossRef Medline
5. Dibner, C., Elias, S., and Frank, D. (2001) XMeis3 protein activity is required for proper hindbrain patterning in *Xenopus laevis* embryos. *Development* **128,** 3415–3426 Medline
6. Machon, O., Masek, J., Machonova, O., Krauss, S., and Kozmik, Z. (2015) Meis2 is essential for cranial and cardiac neural crest development. *BMC Dev. Biol.* **15,** 40 CrossRef Medline
7. Verheije, R., Kupchik, G. S., Isidor, B., Kroes, H. Y., Lynch, S. A., Hawkes, L., Hempel, M., Gelb, B. D., Ghoumid, J., D'Amours, G., Chandler, K., Dubourg, C., Loddo, S., Tümer, Z., Shaw-Smith, C., *et al.* (2019) Heterozygous loss-of-function variants of MEIS2 cause a triad of palatal defects, congenital heart defects, and intellectual disability. *Eur. J. Hum. Genet.* **27,** 278 CrossRef Medline
8. Li, C., Lan, Y., and Jiang, R. (2017) Molecular and cellular mechanisms of palate development. *J. Dent. Res.* **96,** 1184–1191 CrossRef Medline
9. Lane, J., and Kaartinen, V. (2014) Signaling networks in palate development. *Wiley Interdiscip. Rev. Syst. Biol. Med.* **6,** 271–278 CrossRef Medline
10. Suzuki, A., Abdallah, N., Gajera, M., Jun, G., Jia, P., Zhao, Z., and Iwata, J. (2018) Genes and microRNAs associated with mouse cleft palate: a systematic review and bioinformatics analysis. *Mech. Dev.* **150,** 21–27 CrossRef Medline
11. Weatherley-White, R. C., Sakura, C. Y., Jr., Brenner, L. D., Stewart, J. M., and Ott, J. E. (1972) Submucous cleft palate: its incidence, natural history, and indications for treatment. *Plast. Reconstr. Surg.* **49,** 297–304 CrossRef Medline
12. Baek, J.-A., Lan, Y., Liu, H., Maltby, K. M., Mishina, Y., and Jiang, R. (2011) Bmpr1a signaling plays critical roles in palatal shelf growth and palatal bone formation. *Dev. Biol.* **350,** 520–531 CrossRef Medline
13. Pauws, E., Hoshino, A., Bentley, L., Prajapati, S., Keller, C., Hammond, P., Martinez-Barbera, J.-P., Moore, G. E., and Stanier, P. (2009) Tbx22 null mice have a submucous cleft palate due to reduced palatal bone formation and also display ankyloglossia and choanal atresia phenotypes. *Hum. Mol. Genet.* **18,** 4171–4179 CrossRef Medline
14. Yu, L., Gu, S., Alappat, S., Song, Y., Yan, M., Zhang, X., Zhang, G., Jiang, Y., Zhang, Z., Zhang, Y., and Chen, Y. (2005) Shox2-deficient mice exhibit a rare type of incomplete clefting of the secondary palate. *Development* **132,** 4397–4406 CrossRef Medline
15. Xu, J., Wang, L., Li, H., Yang, T., Zhang, Y., Hu, T., Huang, Z., and Chen, Y. (2019) Shox2 regulates osteogenic differentiation and pattern formation during hard palate development in mice. *J. Biol. Chem.* **294,** 18294–18305 CrossRef Medline
16. Ye, W., Song, Y., Huang, Z., Osterwalder, M., Ljubojevic, A., Xu, J., Bobick, B., Abassah-Oppong, S., Ruan, N., Shamby, R., Yu, D., Zhang, L., Cai, C. L., Visel, A., Zhang, Y., *et al.* (2016) A unique stylopod patterning mechanism by Shox2-controlled osteogenesis. *Development* **143,** 2548–2560 CrossRef Medline
17. Uslu, V. V., Petretich, M., Ruf, S., Langenfeld, K., Fonseca, N. A., Marioni, J. C., and Spitz, F. (2014) Long-range enhancers regulating Myc expression are required for normal facial morphogenesis. *Nat. Genet.* **46,** 753–758 CrossRef Medline
18. Gu, S., Wei, N., Yu, X., Jiang, Y., Fei, J., and Chen, Y. (2008) Mice with an anterior cleft of the palate survive neonatal lethality. *Dev. Dyn.* **237,** 1509–1516 CrossRef Medline
19. Scott, A., Hasegawa, H., Sakurai, K., Yaron, A., Cobb, J., and Wang, F. (2011) Transcription factor short stature homeobox 2 is required for proper development of tropomyosin-related kinase B-expressing mechanosensory neurons. *J. Neurosci.* **31,** 6741–6749 CrossRef Medline
20. Louw, J. J., Corveleyn, A., Jia, Y., Hens, G., Gewillig, M., and Devriendt, K. (2015) MEIS2 involvement in cardiac development, cleft palate, and intellectual disability. *Am. J. Med. Genet. A* **167A,** 1142–1146 CrossRef Medline
21. Johansson, S., Berland, S., Gradek, G. A., Bongers, E., de Leeuw, N., Pfundt, R., Fannemel, M., Rødningen, O., Brendehaug, A., and Haukanes, B. I. (2014) Haploinsufficiency of MEIS2 is associated with orofacial clefting and learning disability. *Am. J. Med. Genet. A* **164A,** 1622–1626 CrossRef Medline
22. Giliberti, A., Currò, A., Papa, F. T., Frullanti, E., Ariani, F., Coriolani, G., Grosso, S., Renieri, A., and Mari, F. (2020) MEIS2 gene is responsible for intellectual disability, cardiac defects and a distinct facial phenotype. *Eur. J. Med. Genet.* **63,** 103627 Medline
23. Noda, K., Mishina, Y., and Komatsu, Y. (2016) Constitutively active mutation of ACVR1 in oral epithelium causes submucous cleft palate in mice. *Dev. Biol.* **415,** 306–313 CrossRef Medline
24. Ducy, P., Zhang, R., Geoffroy, V., Ridall, A. L., and Karsenty, G. (1997) Osf2/Cbfa1: a transcriptional activator of osteoblast differentiation. *Cell* **89,** 747–754 CrossRef Medline
25. Welsh, I. C., Hart, J., Brown, J. M., Hansen, K., Rocha Marques, M., Aho, R. J., Grishina, I., Hurtado, R., Herzlinger, D., Ferretti, E., Garcia-Garcia, M. J., and Selleri, L. (2018) Pbx loss in cranial neural crest, unlike in epithelium, results in cleft palate only and a broader midface. *J. Anat.* **233,** 222–242 CrossRef Medline
26. Choi, K. Y., Kim, H. J., Lee, M. H., Kwon, T. G., Nah, H. D., Furuichi, T., Komori, T., Nam, S. H., Kim, Y. J., Kim, H. J., and Ryoo, H. M. (2005) Runx2 regulates FGF2-induced Bmp2 expression during cranial bone development. *Dev. Dyn.* **233,** 115–121 CrossRef Medline
27. Mammadova, A., Zhou, H., Carels, C. E., and Von den Hoff, J. W. (2016) Retinoic acid signalling in the development of the epidermis, the limbs and the secondary palate. *Differentiation* **92,** 326–335 CrossRef Medline
28. Fakhouri, W. D., Metwalli, K., Naji, A., Bakhiet, S., Quispe-Salcedo, A., Nitschke, L., Kousa, Y. A., and Schutte, B. C. (2017) Intercellular genetic interaction between Irf6 and Twist1 during craniofacial development. *Sci. Rep.* **7,** 7129 CrossRef Medline
29. Choe, S.-K., Ladam, F., and Sagerström, C. G. (2014) TALE factors poise promoters for activation by Hox proteins. *Dev. Cell* **28,** 203–211 CrossRef Medline
30. Huang, H., Rastegar, M., Bodner, C., Goh, S.-L., Rambaldi, I., and Featherstone, M. (2005) MEIS C termini harbor transcriptional activation domains that respond to cell signaling. *J. Biol. Chem.* **280,** 10119–10127 CrossRef Medline
31. Joo, S., Wang, M. H., Lui, G., Lee, J., Barnas, A., Kim, E., Sudek, S., Worden, A. Z., and Lee, J.-H. (2018) Common ancestry of heterodimerizing TALE homeobox transcription factors across Metazoa and Archaeplastida. *BMC Biol.* **16,** 136 CrossRef Medline
32. Sun, C., Zhang, T., Liu, C., Gu, S., and Chen, Y. (2013) Generation of Shox2-Cre allele for tissue specific manipulation of genes in the developing heart, palate, and limb. *Genesis* **51,** 515–522 CrossRef Medline
33. Danielian, P. S., Muccino, D., Rowitch, D. H., Michael, S. K., and McMahon, A. P. (1998) Modification of gene activity in mouse embryos *in utero* by a tamoxifen-inducible form of Cre recombinase. *Curr. Biol.* **8,** 1323–1326 CrossRef Medline
34. Muzumdar, M. D., Tasic, B., Miyamichi, K., Li, L., and Luo, L. (2007) A global double-fluorescent Cre reporter mouse. *Genesis* **45,** 593–605 CrossRef Medline
35. Wang, J., Bai, Y., Li, N., Ye, W., Zhang, M., Greene, S. B., Tao, Y., Chen, Y., Wehrens, X. H., and Martin, J. F. (2014) Pitx2-microRNA pathway that delimits sinoatrial node development and inhibits predisposition to atrial fibrillation. *Proc. Natl. Acad. Sci. U.S.A.* **111,** 9181–9186 CrossRef Medline

36. Wang, F., Flanagan, J., Su, N., Wang, L.-C., Bui, S., Nielson, A., Wu, X., Vo, H.-T., Ma, X.-J., and Luo, Y. (2012) RNAscope: a novel *in situ* RNA analysis platform for formalin-fixed, paraffin-embedded tissues. *J. Mol. Diagn.* **14,** 22–29 CrossRef Medline
37. Zhang, Z., Yu, X., Zhang, Y., Geronimo, B., Lovlie, A., Fromm, S. H., and Chen, Y. (2000) Targeted misexpression of constitutively active BMP receptor-IB causes bifurcation, duplication, and posterior transformation of digit in mouse limb. *Dev. Biol.* **220,** 154–167 CrossRef Medline
38. Kim, D., Langmead, B., and Salzberg, S. L. (2015) HISAT: a fast spliced aligner with low memory requirements. *Nat. Methods* **12,** 357–360 CrossRef Medline
39. Liao, Y., Smyth, G. K., and Shi, W. (2014) featureCounts: an efficient general purpose program for assigning sequence reads to genomic features. *Bioinformatics* **30,** 923–930 Medline
40. Love, M. I., Huber, W., and Anders, S. (2014) Moderated estimation of fold change and dispersion for RNA-Seq data with DESeq2. *Genome Biol.* **15,** 550 CrossRef Medline
41. Yu, G., Wang, L.-G., Han, Y., and He, Q.-Y. (2012) clusterProfiler: an R package for comparing biological themes among gene clusters. *OMICS* **16,** 284–287 CrossRef Medline
42. Daum, J. M., Keles, Ö., Holwerda, S. J., Kohler, H., Rijli, F. M., Stadler, M., and Roska, B. (2017) The formation of the light-sensing compartment of cone photoreceptors coincides with a transcriptional switch. *Elife* **6,** e31437 CrossRef Medline
43. Langmead, B., and Salzberg, S. L. (2012) Fast gapped-read alignment with Bowtie 2. *Nat. Methods* **9,** 357–359 CrossRef Medline
44. Ramírez, F., Ryan, D. P., Grüning, B., Bhardwaj, V., Kilpert, F., Richter, A. S., Heyne, S., Dündar, F., and Manke, T. (2016) deepTools2: a next generation web server for deep-Sequencing data analysis. *Nucleic Acids Res.* **44,** W160-W165 CrossRef Medline
45. Zhang, Y., Liu, T., Meyer, C. A., Eeckhoute, J., Johnson, D. S., Bernstein, B. E., Nusbaum, C., Myers, R. M., Brown, M., Li, W., and Liu, X. S. (2008) Model-based analysis of ChIP-Seq (MACS). *Genome Biol.* **9,** R137 CrossRef Medline
46. Ross-Innes, C. S., Stark, R., Teschendorff, A. E., Holmes, K. A., Ali, H. R., Dunning, M. J., Brown, G. D., Gojis, O., Ellis, I. O., Green, A. R., Ali, S., Chin, S. F., Palmieri, C., Caldas, C., and Carroll, J. S. (2012) Differential oestrogen receptor binding is associated with clinical outcome in breast cancer. *Nature* **481,** 389–393 CrossRef Medline